2008 8th IEEE-RAS International Conference on Humanoid Robots
December 1 ~ 3, 2008 / Daejeon, Korea

Vibration Damping Control of Robot Arm Intended for Service Application in Human Environment

Dzmitry Tsetserukou, Naoki Kawakami, Susumu Tachi

University of Tokyo, Japan, dima_teterukov@ipc.i.u-tokyo.ac.jp, {kawakami, tachi}@star.t.u-tokyo.ac.jp

***Abstract*— The paper focuses on vibration damping control of a new anthropomorphic robot arm enabling the torque measurement in each joint and tactile area recognition to ensure safety while performing tasks of physical interaction with environment or human beings. The vibrations in heavily loaded joints have risen due to compliances introduced into each joint of the robot arm by means of torque sensors. Such oscillations deteriorate the performance of the manipulator and present undesirable disturbance during interaction with human beings. In order to overcome this disadvantage we have proposed robust technique allowing considerable reduction of the oscillation amplitude through acceleration signal feedback. The detailed design procedure of the lead controller enabling improvement of transient response is presented in the paper. The experimental results of vibration damping control show the feasibility of proposed approach to suppress the oscillations of compliant robot joint.**

I. Introduction

The service robotics aimed at assistance to human in everyday life environment is nowadays gaining increased interest of researchers and industry. Such robots are programmed to perform continuously changing tasks in unstructured human being environment. Both coexistence, when the human and robot share the same workspace, and cooperation, when the human and robot work on the same task, impose strict requirements on manipulator behavior and control in order to ensure safe interaction with environment, effectiveness of target task execution, and ergonomic cooperation.

Several effective collision avoidance strategies were developed. For instance, the high-speed vision system attached to the robot arm allows real-time collision avoidance [1]. Is should be noted, that such tasks under human supervision as transporting the object, leading the robot tip via force-following, performing the assembling tasks, require the processing algorithm of contact state. Generally, two techniques of safe interaction with robot are well recognized, namely, passive compliance control and active force control.

Whereas the mechanical leaf springs [2] and variable stiffness actuators [3] integrated into each joint allow achieving fast response to external disturbance, they also cause vibrations destabilizing the dynamic behavior. Additionally, the robot control in such cases is complicated by many unknown parameters (e.g. actuator stiffness and damping). Another approach to improvement of the intrinsic safety of robot is to reduce the weight of components. The main drawback of this method is occurrence of undamped structural vibrations.

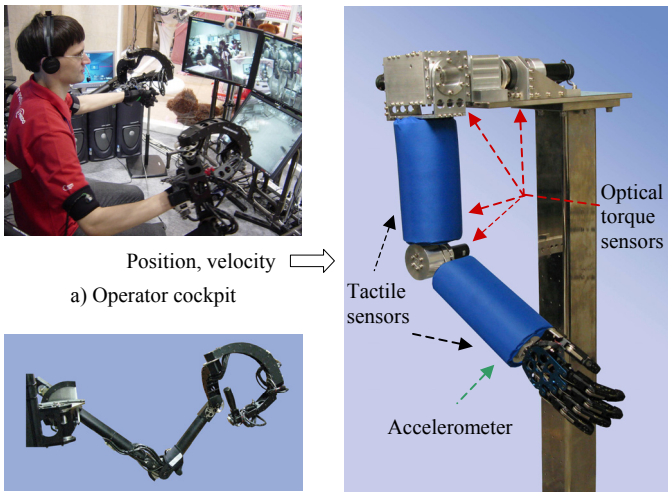

Fig. 1 Robot teleoperation system

Active force control implies that the robot structure is stiff enough to provide high position accuracy; and contact ability with environment is achieved by excessive sensory system feedback [4]. However, due to the time lag induced by sampling process, such robots pose dangerousness at the moment of impact.

To realize the safe physical contact of entire robot arm structure with human and to guarantee the collision avoidance, we developed a whole-sensitive robot arm (by using artificial skin and distributed torque sensors in each joint [5]). When contact with environment occurs, manipulator automatically generates compliant motion according to the measured external force vector (active control). Thus, the whole structure of the manipulator can safely interact with an unstructured environment. The newly developed anthropomorphic manipulator having 4-DOF arm and 8-DOF hand (Fig. 1(c)) is capable of safe interaction with environment wherever contact occurs on the arm surface [6]. The torque sensors introduce compliances, which soften the impact forces on the initial state of contact transient (passive control). The teleoperated robot arm is controlled by operator's motion (Fig. 1(a)). During operation of manipulator the movement information (position, orientation, and velocity) is acquired through encoders of the motors installed into each joint of the master arm (Fig. 1(b)). The motion of the elbow is controlled by the tilt sensor.

978-1-4244-2822-9/08/$25.00 ©2008 IEEE

On the other hand, joint flexibility increases the vibration during acceleration and deceleration stages because of inertial loading. Thus, the main goal of this paper is elaboration of the vibration damping control algorithm to achieve the smooth continuous motion while interacting with environment.

The remainder of the paper is structured as follows. Section 2 introduces the mathematical model of the robot joint with flexibility, and method for oscillation parameter identification. The lead compensator design algorithm is presented in Section 3. The experimental results are given in Section 4. In Section 5, we briefly conclude the paper and discuss the future work.

II. The Model of Robot with Joint Flexibility

A. Dynamic Model of Flexible Robot Joint

Flexibility introduced into robot arm joint through harmonic drive and torque sensors changes the dynamic behavior of mechanical structure. Robot joint with compliance can be represented as three-inertia system (Fig. 2) including: (1) the inertias of motor J_m, harmonic drive output shaft J_D, and load J_L; (2) the spring elements of harmonic drive (with torsional stiffness k_1) and torque sensor (with torsional stiffness k_2).

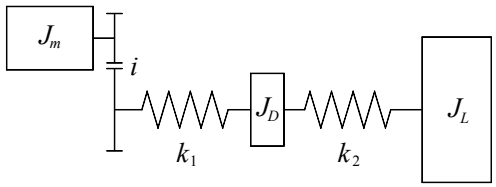

Fig. 2 3-DOF vibration system

Due to neglible value of inertia of output shaft of harmonic drive, three-inertia model can be reduced to the equivalent two-DOF one with mass inertias i^2J_m and J_L (Fig. 3).

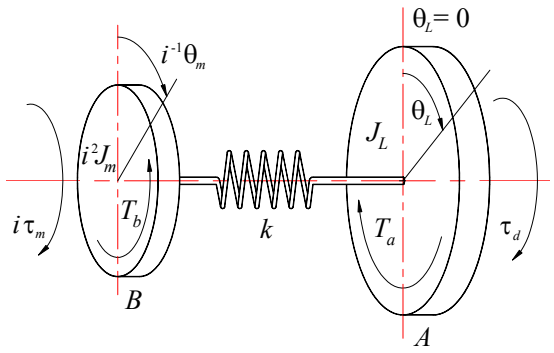

Fig. 3 Equivalent 2-DOF vibration system

The torsional stiffnesses k_1, k_2, and equivalent spring constant k_e derived from Eq. (1) are listed in Table 1.

$$\frac{1}{k_e} = \frac{1}{k_1} + \frac{1}{k_2}, \quad k = k_e = \frac{k_1 k_2}{k_1 + k_2}. \tag{1}$$

TABLE I
Torsional Stifnesses of Robot Joints

Parameters	Arm joints			
	Shoulder			Elbow
	J1, Pitch	J2, Roll	J3, Yaw	J4, Pitch
Torsional stiffness of harmonic drive k_1, [kNm/rad]	6.1	6.1	3.33	3.33
Torsional stiffness of the torque sensors k_2, [kNm/rad]	3.23	2.73	0.95	0.95
Equivalent torsional stiffness k_e, [kNm/rad]	2.112	1.886	0.739	0.739

The dynamic equations of the n-DOF manipulator with joint compliance in joint space coordinates can be obtained by D'Alembert's principle. The equations of static equilibrium for mass A (Eq. (2)) and mass B (Eq. (3)) ignoring damping are as follows:

$$\begin{cases} J_L(\theta_L)\ddot{\theta}_L = k\left(i^{-1}\theta_m - \theta_L\right) + \tau_d & (2) \\ J_m\ddot{\theta}_m = -i^{-1}k\left(i^{-1}\theta_m - \theta_L\right) + \tau_m & (3) \\ \tau_d = \tau_{EXT} - G(\theta_L) - C(\theta_L, \dot{\theta}_L)\dot{\theta}_L & (4) \\ \tau = k\left(i^{-1}\theta_m - \theta_L\right), & (5) \end{cases}$$

where $\theta_L, \dot{\theta}_L, \ddot{\theta}_L \in R^n$ are the vectors of the link angles, the link angular velocities, and the link angle accelerations, respectively; $\theta_m, \ddot{\theta}_m \in R^n$ are the vectors of motor angles, and the motor angle accelerations, respectively; $k \in R^{n\times n}$ is the diagonal matrix of joint stiffness; $i \in R^n$ is the vector of gear reduction ratios; $J_L(\theta_L) \in R^{n\times n}$ is the symmetric, positive definite link inertia matrix; $J_m \in R^{n\times n}$ is the diagonal, positive definite rotor inertia matrix; $\tau_d \in R^n$ is the vector of disturbance torques; $\tau_m \in R^n$ is the vector of torques applied by motor; $\tau_{EXT} \in R^n$ is the vector of applied external joint torques; $G(\theta_L) \in R^n$ is the vector of gravitational torques; $C(\theta_L, \dot{\theta}_L) \in R^n$ represents the vector of Coriolis and centrifugal torques; $\tau_m \in R^n$ is the vector of torques applied by motor; the torque in the shaft $\tau \in R^n$ is directly proportional to twist angle $\theta = (i^{-1}\theta_m - \theta_L)$.

The transfer function of two-mass robot joint can be deduced from Eq. (2)-(5) and has the block diagram presentation shown in Fig. 4. To provide the faithful tracing of the motion of operator arm and to generate desired compliant trajectory while interaction with environment, each joint has PD control loop shown in Fig. 5 (where $\theta_{md}, \dot{\theta}_{md}$ are the desired angle and angular speed; K_p, K_v are proportional and derivative gains). The under-dumped response of motor dynamics can be easily derived through PD gains adjustment. However, there is no feedback signal from load position to enable control of the unbalanced inertial loading dynamics.

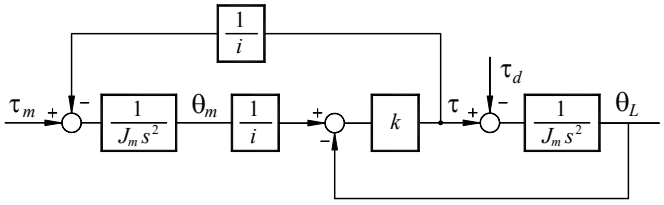

Fig. 4 Block diagram of two-mass robot joint

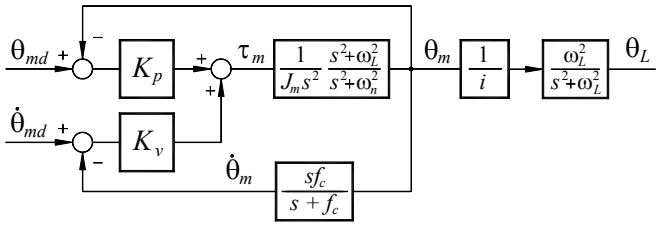

Fig. 5 Block diagram of two-mass robot joint with PD

The natural frequency of two-mass system ω_n and natural frequency of one-mass robot joint ω_L are derived from the following equations:

$$\omega_n = \sqrt{k\left(\frac{1}{i^2 J_m} + \frac{1}{J_L}\right)}, \qquad \omega_L = \sqrt{\frac{k}{J_L}}. \tag{6}$$

The experimental results of human-robot interaction for the first joint show that despite the smooth trajectory (Fig. 6(a)) generated by the admittance controller according to the sensed joint torque, the vibratory behavior is recorded by torque sensor (Fig. 6(b)).

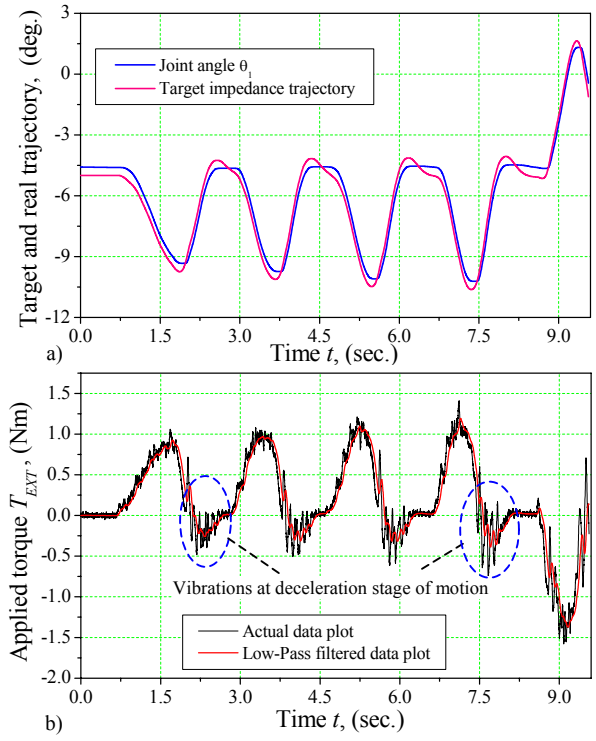

Fig. 6 Experimental results of human-robot interaction

Several techniques were proposed to attenuate vibrations by using negative torque feedback [7], [8]. The idea behind this approach is that negative torque feedback reduces the effective inertia of the motor rotor in (K_T+1) times, where K_T is the torque gain. However, whereas this approach can suppress the vibrations to some extent, it cannot control the main source of vibrations, namely, the inertial loading.

B. Oscillation Parameter Identification

The approach proposed by us is to employ position feedback based on information from accelerometer and lead controller to improve the damping property of the compliant robot joint. To illustrate the torsional vibrations caused by unbalanced inertial load (see the open-loop block of diagram in Fig. 5), let us consider dynamic model of robot arm given in Fig. 7.

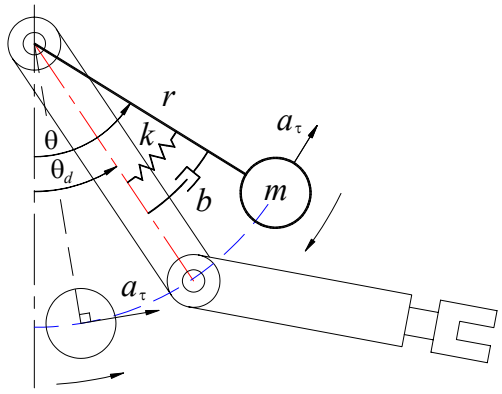

Fig. 7 Graphical presentation of torsional vibrations

The desired trajectory generated by master arm movement or, in case of interaction with environment by admittance controller, is described by angle θ_d. The flexibility of the joint produces vibrations about *Z*-axis of corresponding joint. Using the balance equations of forces acting on the joint we can write:

$$J_L\ddot{\theta}_L + b\dot{\theta}_L + k\left(\theta_L - \theta_d\right) = 0, \tag{7}$$

where $\theta_L, \dot{\theta}_L, \ddot{\theta}_L$ are actual angle, angular speed and angular acceleration of the link, respectively; b is a viscous damping constant. We can neglect the influence of gravitational force due to small vibration angle change.

By Laplace transform we get the following transfer function:

$$\frac{\theta_L(s)}{\theta_d(s)} = \frac{k}{J_L s^2 + bs + k} = \frac{\omega_L^2}{s^2 + 2\zeta\omega_L s + \omega_L^2}, \tag{8}$$

where ζ is the damping coefficient which can be derived from the following equation:

$$\zeta = \frac{b}{2\sqrt{kJ_L}}. \tag{9}$$

The oscillation periods of the angle of link, angular acceleration, and angular speed are identical. Therefore, from analysis of the angular acceleration signal we can obtain the unknown parameters of the joint, namely: natural frequency and damping coefficient. The linear tangential acceleration a_τ can be measured by accelerometer. Then, the corresponding angular acceleration is given by:

$$\alpha = a_\tau / r, \tag{10}$$

where r is the radius of curvature or distance to the accelerometer (in our case it equals 0.241 m).

The three-axis accelerometer with sensitivity of 600 mV/G was used. The special plastic case was manufactured in order to fixedly attach the body of the sensor to the tip of forearm. The model of accelerometer attachment along with coordinate systems associated with robot elbow joint and sensor are given in Fig. 8.

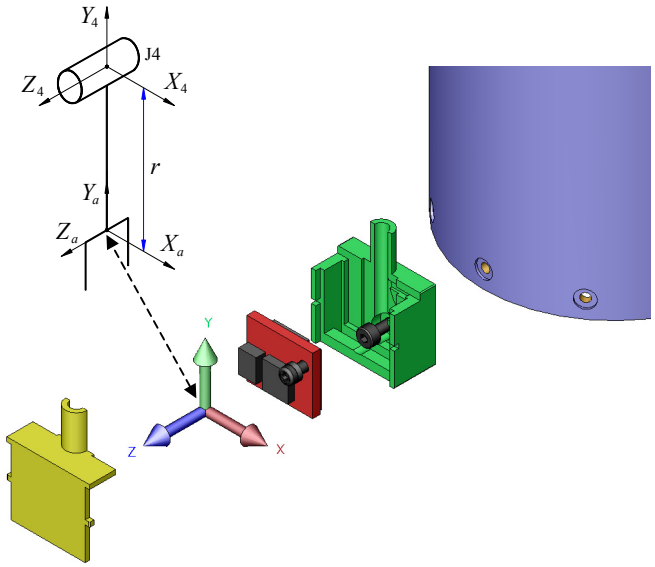

Fig. 8 Accelerometer attachment scheme

As seen from Fig. 8, the angular acceleration corresponds to the X component of the accelerometer output. During experiment, elbow joint was fixedly mounted, and the impulse force was applied to the tip of the robot forearm. The vibrations were visually observed. Fig. 9 shows the recorded acceleration curve. To eliminate high frequency noise, the digital low-pass filter was deployed with cut-off frequency of 100 Hz.

The procedure of oscillation parameter determination is presented below.

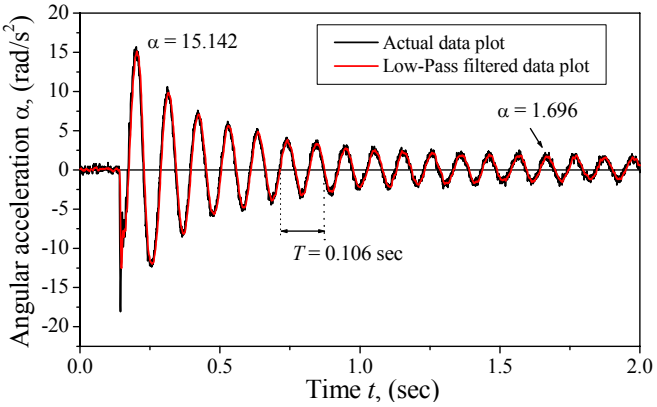

Fig. 9 Angular acceleration plot

The damping coefficient can be calculated from:

$$\zeta = \frac{\delta}{\sqrt{4\pi^2 + \delta^2}}, \tag{11}$$

where δ is the logarithmic decrement expressed by:

$$\delta = \frac{1}{m} \ln\left(\frac{\alpha_n}{\alpha_{n+m}}\right), \tag{12}$$

where α_n, α_{n+m} are the measured amplitudes of angular acceleration; m is the number of peaks over which the amplitude change is measured [9].

To estimate the logarithmic decrement reliably, the number of peaks was assigned to 14. The calculated value of logarithmic decrement δ is 0.1564, and damping coefficient ζ is equal to 0.0249 that indicates that system is lightly damped.

The damped natural angular frequency ω_d is given by:

$$\omega_d = \frac{2\pi}{T} = \frac{2\pi}{0.106} = 58.28 \text{ rad/sec}. \tag{13}$$

Then, the natural angular frequency is calculated as:

$$\omega_L = \frac{\omega_d}{\sqrt{1-\zeta^2}} = \frac{58.28}{\sqrt{1-0.0249^2}} = 58.3 \text{ rad/sec}. \tag{14}$$

After substitution of calculated parameters into Eq. (8), the transfer function becomes:

$$\frac{\theta_L(s)}{\theta_d(s)} = \frac{3398.9}{s^2 + 2.903s + 3398.9}. \tag{15}$$

To reduce the lightly damped vibrations, the oscillation-damping controller is, therefore, needed.

III. Design of Vibration Damping Controller

We are proposing to use load angle position feedback and lead compensator to damp the undesirable vibrations. The angular position can be calculated from accelerometer data by

means of double integration. The high-pass filtering is necessary to eliminate the drift of the signal (Fig. 10). The cut-off angular frequency was assigned to 3 rad/sec.

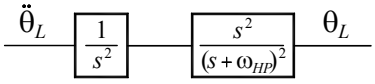

Fig. 10 Diagram of acceleration processing

The transfer function is expressed as:

$$\frac{y(s)}{u(s)}=\frac{\theta_L(s)}{\ddot{\theta}_L(s)}=\frac{1}{s^2}\frac{s^2}{\left(s+\omega_{HP}\right)^2}=\frac{1}{\left(s+\omega_{HP}\right)^2}. \tag{16}$$

State-space presentation is described by:

$$\begin{bmatrix}\dot{\theta}_L(t)\\ \dot{v}(t)\end{bmatrix}=\begin{bmatrix}0 & 1\\ -\omega_{HP}^2 & -2\omega_{HP}\end{bmatrix}\begin{bmatrix}\theta_L(t)\\ v(t)\end{bmatrix}+\begin{bmatrix}0\\ 1\end{bmatrix}u(t) \tag{17}$$

$$y(t)=\begin{bmatrix}1 & 0\end{bmatrix}\begin{bmatrix}\theta_L(t)\\ v(t)\end{bmatrix}, \tag{18}$$

where $v=\dot{\theta}_L$ is state variable; the input of the system *u(t)* is the signal from accelerometer; and *y(t)* is the output signal. To implement program code we have to use the discrete presentation of the functions with sampling time of *T*. For calculation step *k* we have:

$$\begin{bmatrix}\theta_{L(k+1)}\\ \dot{\theta}_{L(k+1)}\end{bmatrix}=A_d\begin{bmatrix}\theta_{L(k)}\\ \dot{\theta}_{L(k)}\end{bmatrix}+B_dU_{(k)} \tag{19}$$

$$y_{(k)}=\theta_{L(k)}. \tag{20}$$

The matrices A_d and B_d are given by:

$$A_d=\begin{bmatrix}e^{-\omega_{HP}T}+\omega_{HP}Te^{-\omega_{HP}T} & Te^{-\omega_{HP}T}\\ -\omega_{HP}^2Te^{-\omega_{HP}T} & e^{-\omega_{HP}T}+\omega_{HP}Te^{-\omega_{HP}T}\end{bmatrix} \tag{21}$$

$$B_d=\begin{bmatrix}\left(-e^{-\omega_{HP}T}-\omega_{HP}Te^{-\omega_{HP}T}+1\right)\big/\omega_{HP}^2\\ Te^{-\omega_{HP}T}\end{bmatrix}. \tag{22}$$

To improve the system performance and to meet the performance specification, we should design the compensator. Such properties of lead compensator as speeding the response up and increasing the stability of the system make it the preferable one. The compensator contributes a phase lead at existing gain crossover frequency. The transfer function of lead compensator [10] is written as:

$$G_c(s)=\frac{K}{\alpha}\frac{\left(s+\omega_z\right)}{\left(s+\omega_p\right)}=\frac{K}{\alpha}\frac{\left(s+\omega_z\right)}{\left(s+\omega_z/\alpha\right)}, \tag{23}$$

where ω_z, ω_p are the zero and pole; *K* is the constant gain.

The block diagram of the closed loop system with lead compensator is shown in Fig. 11.

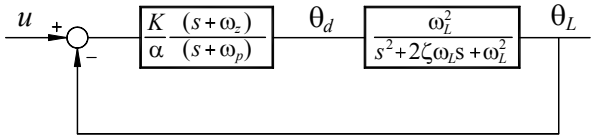

Fig. 11 System with lead compensator

First, we determine the gain *K* to satisfy the steady-state error e_{ss} (less then 1.0 % for a unit step function):

$$e_{ss}=\frac{1}{1+G_c(0)G(0)}\le 0.01. \tag{24}$$

The calculated value of *K* is 99. The specification of system damping coefficient of 0.55 provides the value of required phase margin ϕ defined by:

$$\phi=\tan^{-1}\frac{2\zeta}{\sqrt{-2\zeta^2+\sqrt{1+4\zeta^2}}}. \tag{25}$$

The derived phase margin ϕ is 55.7°. Value of the uncompensated system phase margin is as low as 0.29°. Therefore, we need to add phase lead, which satisfies required damping property of the system. With account of compensation of shift in the gain crossover frequency the maximum required phase lead angle ϕ_{max} is approximately 60°. The coefficient α is computed from:

$$\alpha=\frac{1-\sin(\phi_{\max})}{1+\sin(\phi_{\max})}. \tag{26}$$

The new gain crossover frequency ω_c for total compensated system is given by intersection of line $20\log_{10}\sqrt{a}$ and bode magnitude plot (for α of 0.0718, ω_c=-11.44 dB). The final step is to calculate corner frequencies ω_z, ω_p. Taking advantage of the fact that the maximum phase lead angle ϕ_{max} occurs at the geometric mean of two corner frequencies ω_z, ω_p, we can get:

$$\omega_z=\omega_c\sqrt{\alpha}, \qquad \omega_p=\omega_c\big/\sqrt{\alpha}. \tag{27}$$

The values of ω_z and ω_p equal 321 rad/sec and 4477. Using the above mentioned procedure, the discrete presentation of the lead compensator with sampling time of *T* is:

$$x_{(k+1)}=e^{-\omega_pT}x_{(k)}+\left(\left(1-e^{-\omega_pT}\right)\big/\omega_p\right)U_{c(k)} \tag{28}$$

$$y_{(k)}=\theta_{d(k)}=(\omega_z-\omega_p)x_{(k)}+U_{c(k)}, \tag{29}$$

where $U_{c(k)}$ is the discrete input signal.

The obtained value of desired load angle θ_d is then processed by PD control loop. The magnitude curve and phase-angle curve for the compensated system are shown in Fig. 12. The phase and gain margins are 60 deg. and $+\infty$, respectively. Therefore, compensated system meets both the steady-state and the relative stability requirements.

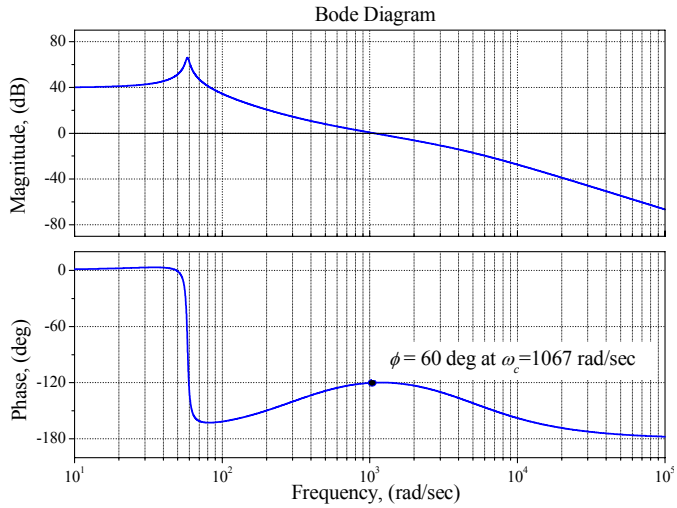

Fig. 12 Bode diagram

Thus, the desirable transient behavior was achieved through usage of lead compensator. To verify the theory and to evaluate the feasibility and performance of the proposed damping controller, the experiment was conducted.

IV. Experiment and Discussion

During the experiment the impulse force was applied to the tip of the forearm, and the acceleration signal with desired angle was recorded (Fig. 13).

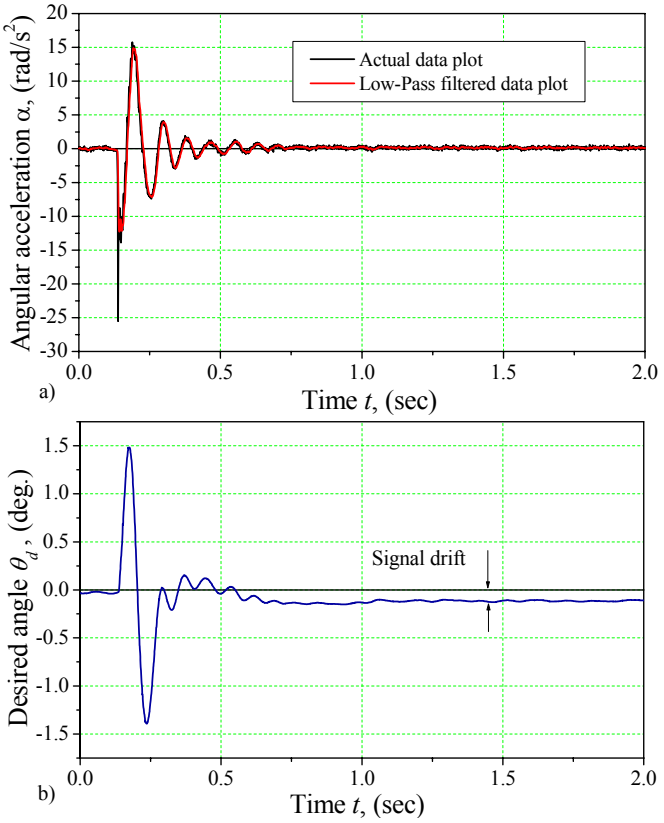

Fig. 13 Experimental results

The experimental results show the successful damping of oscillation magnitude. As follows from Fig. 13(b), the system resists the quick change in angular speed, and, therefore, provides more smooth dynamic behavior. It is important to emphasize here, that theoretically calculated control gain and feedback gain must be adjusted while experiment conducting. Too high gains can cause increasing sensitivity to noise signal. The signal drift presented in Fig. 13(b) is generated by small change in angular balance position.

V. Conclusion and Future Research

The flexibility of robot joint caused by compliant elements, such as torque sensors, harmonic drives, and lightweight mechanical connectors, produce significant effect on the dynamics of robot. The presented experimental results prove oscillatory behavior of joints of whole sensitive robot arm.

To compensate flexibility effect, first, we elaborated the dynamic model of the robot joint as two-mass system. The system with lead compensator and angular position of the load feedback is proposed to dump undesired vibrations. The oscillation parameters required to design the lead controller were determined by using experimental data and analytical equations. The experimental results show high performance of the developed controller in terms of successful damping of vibrations. In the future research we will address the tasks of implementation of vibration damping in each robot joint and realization of adaptive compensator to adjust parameters according to the effective inertia.

Acknowledgment

The research is supported in part by a Japan Society for the Promotion of Science (JSPS) Postdoctoral Fellowship for Foreign Scholars.

References

[1] S. Morikawa, T. Senoo, A. Namiki, and M. Ishikawa, "Real-time collision avoidance using a robot manipulator with light-weight small high-speed vision system" in *Proc. ICRA'07*, 2007, pp. 794-799.

[2] H. Iwata, S. Kobashi, T. Aono, and S. Sugano, "Design of anthropomorphic 4-DOF tactile interaction manipulator with passive joints," in *Proc. IROS'05*, 2005, pp. 1785-1790.

[3] A. Bicchi and G. Tonietti, "Fast and soft arm tactics: dealing with the safety-performance trade-off in robot arms design and control," *IEEE Robotics and Automation Magazine*, vol.11, no.2, pp. 22-33, June 2004.

[4] M.A. Diftler, C. J. Culbert, R. O. Ambrose, Jr. R. Platt, and W. J. Bluethmann, "Evolution of the NASA/DARPA Robonaut control system," in *Proc. ICRA'03*, 2003, pp. 2543-2548.

[5] D. Tsetserukou, R. Tadakuma, H. Kajimoto, and S. Tachi, "Optical torque sensors for local impedance control realization of an anthropomorphic robot arm," *Journal of Robotics and Mechatronics*, vol.18, no.2, pp.121-130, April 2006.

[6] D. Tsetserukou, R. Tadakuma, H. Kajimoto, N. Kawakami, and S. Tachi, "Intelligent variable joint impedance control and development of a new whole-sensitive anthropomorphic robot arm," in *Proc. CIRA'07*, 2007, pp. 338-343.

[7] G. Zhang and J. Furusho, "Control of robot arms using joint torque sensors," in *Proc. ICRA'97*, 1997, pp. 3148-3153.

[8] A. Albu-Schaffer and G. Hirzinger, "State feedback controller for flexible joint robots: A globally stable approach implemented on DLR`s light weight robots," in *Proc. IROS'00*, 2000, pp. 1087-1093.

[9] J. B. Hartman, *Dynamics of Machinery*. New York, USA: McGraw-Hill, 1956.

[10] K. Ogata, *Modern Control Engineering*. Upper Saddle River, NJ, USA: Prentice-Hall, 1997.